RNA Aptamers to *S*-Adenosylhomocysteine: Kinetic Properties, Divalent Cation Dependency, and Comparison with Anti-*S*-adenosylhomocysteine Antibody†

Kirsti Gebhardt,* Afshin Shokraei, Eshrat Babaie, and Bjørn H. Lindqvist

Biotechnology Centre of Oslo, University of Oslo, P.O. Box 1125 Blindern, 0317 Oslo, Norway

Received February 8, 2000; Revised Manuscript Received April 4, 2000

ABSTRACT: To explore the potential of RNA aptamers as small-molecule discriminating devices, we have characterized the properties of aptamers selected from a library of approximately 10^{14} variants through their interaction with *S*-adenosylhomocysteine (SAH, AdoHcy). Competition studies with SAH and azaSAM analogues revealed that the Hoogsteen face of adenine is the main contributor to binding, whereas specificity for SAH is conferred by a secondary contact point at or near the sulfur/thioether of homocysteine (Hcy). Binding specificities were determined by both affinity chromatography and a novel method designed for the biosensor. The kinetic properties of individual aptamers, including the "classic" ATP aptamer that also emerged in our selection, were studied by biosensor analysis. Association rates were slow, but the complexes were stable, suggesting micro- to submicromolar affinities. A solution affinity of ~0.1 μM was found for the strongest binding variant under the conditions used for selection (5 mM Mg^{2+}). Systematic studies of the effect of Mg^{2+} and Mn^{2+} on binding, however, revealed that the affinity of the aptamers could be substantially improved, and at optimized conditions of Mn^{2+} the affinity of one of the aptamers approached that of an anti-SAH antibody with similar/identical binding specificity. Comparisons with the MAb suggest that the on rate is the limiting factor for high-affinity binding by these aptamers, and comparison with a truncated aptamer shows that shortening of RNA constructs may alter binding kinetics as well as sensitivity to ions.

The potentials of in vitro selected RNA ligands (aptamers) as small-molecule discriminating devices are currently being explored (reviewed in refs *1* and *2*). The SELEX procedure (systematic evolution of ligands by exponential enrichment; *3)* has been used to isolate RNA variants from large pools of $10^{14}-10^{15}$ randomized sequences that can discriminate between closely related compounds such as, e.g., caffeine and theophylline with a discrimination factor of more than 10 000 (*4*). Most aptamers recognizing low-molecular weight compounds have moderate to high affinities for their targets with dissociation constants (K_ds) in the submicro- to nanomolar range (*1*). So far, the highest affinity achieved is a K_d of 0.77 nM for an aptamer recognizing the aminoglycoside antibiotic tobramycin (*5*). For larger targets such as proteins, the affinities and specificities of aptamers may rival or even surpass that of antibodies (*6*).

S-adenosylhomocysteine (SAH,[1] AdoHcy) is a key intermediate in the metabolism of the amino acid methionine (*7*−*9*). It is formed from *S*-adenosylmethionine (SAM, AdoMet) following methyl group transfer to a suitable acceptor molecule. SAH is a potent inhibitor of this reaction, and thus the level of SAH is critically linked to cellular methylation state. SAH is also the direct and only source of the potentially toxic compound homocysteine (Hcy), the product of SAH degradation in addition to adenosine (Ado). Elevated total Hcy (the sum of the free and protein-bound forms) in plasma or serum is used as a diagnostic marker of certain forms of cardiovascular disease (*10*).

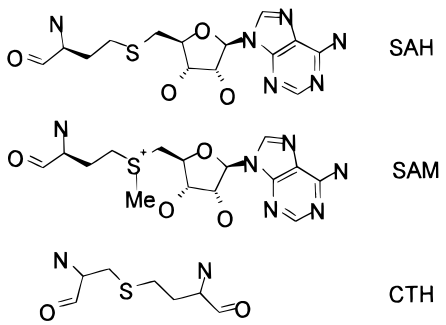

FIGURE 1: Structures of SAH, SAM, and CTH.

SAH is a low molecular mass compound (384 Da), consisting of the nucleoside Ado joined by a 5' thioether linkage to the amino acid Hcy (Figure 1). Previous SELEX experiments targeting Ado-containing cofactors have identified two classes of RNA motifs that recognize either the Ado (*11*) or the adenine (*12*) portion of these molecules. The

† This research was supported by The Norwegian Research Council, Grant 111472/310.

* To whom correspondence should be addressed: phone +47 22 95 85 21, fax: +47 22 69 41 30, e-mail kgebhard@embnet.uio.no. Other authors: A.S., phone +47 22 95 84 58, fax +47 22 69 41 30, e-mail afshins@biotek.uio.no; E.B., phone +47 22 95 84 58, fax +47 22 69 41 30, e-mail esbabaie@biotek.uio.no; B.H.L., phone +47 22 85 45 98, fax +47 22 69 41 30; e-mail b.h.lindqvist@bio.uio.no.

[1] Abbreviations: K_d, equilibrium dissociation constant; k_a, association rate constant; k_d, dissociation rate constant; Ado, adenosine; Ade, adenine; SAH, *S*-adenosylhomocysteine; SAM, *S*-adenosylmethionine; SAC, *S*-adenosylcysteine; CTH, cystathionine; FMN, flavin mononucleotide; FAD, flavin adenine dinucleotide; nt, nuclotide; ss, single-stranded; ds, double-stranded; bp, base pair; MAb, monoclonal antibody; PCR, polymerase chain reaction.

10.1021/bi000295t CCC: $19.00
Published on Web 05/19/2000

"ATP aptamer" binds the Ado moiety of ATP and AMP with submicromolar affinity (K_d 0.7 μM in solution; *11)* and has emerged in selections to such different targets as ATP (*11*), NAD^+ (*13*), and SAM (*14*). The repeated isolation of this motif illustrates both the reproducibility of SELEX and the fact that the ATP aptamer does not discriminate between the various substitutents at the 5′ position (*14*). The adenine-specific aptamers emerged in a selection to coenzyme A (CoA), and neither in this case was there any apparent interaction with the 5′ moiety *(12)*. So far, only the FMN aptamer isolated in a selection to FAD (*13)* has been shown to recognize the 5′ substituent of an Ado cofactor, although in this case binding was exclusively directed toward the 5′ FMN group. Aptamers with specificity for the amino acids arginine, citrulline, tryptophane/phenylalanine, valine, and isoleucine have been obtained by SELEX. The affinities of these interactions range from millimolar for Val and Trp/Phe (*15, 16*), to micromolar for Ile (*17*), citrulline (*18*), and Arg (*19*). By use of more stringent selection criteria, the affinity for Arg could be increased nearly 200-fold (*20*).

In this study we report the isolation and characterization of aptamers with specificity for SAH. The selection process resulted in the identification of a novel, predominantly adenine-recognizing motif, which in contrast to previously isolated Ado/adenine-recognizing aptamers also makes a contact with the substitutent at the 5′ position, in this case Hcy. The binding of aptamers to immobilized SAH was monitored in real time in a biosensor to provide information on association and dissociation kinetics. Biosensor analysis was also used to measure the affinity of the aptamers for immobilized and soluble SAH and to study the effects of the divalent cations Mg^{2+} and Mn^{2+} on binding. A method for mapping of binding specificities in the biosensor was developed and compared to the results from analytical affinity chromatography. Finally, the availability of an anti-SAH monoclonal antibody with similar (or identical) binding specificity as the SAH aptamer allowed direct comparisons of antibody and aptamer kinetics and affinity.

EXPERIMENTAL PROCEDURES

Materials. Fine chemicals, except 5′-thiodeoxymethyladenosine (Fluka) and adenosine triphosphate (Boehringer Mannheim), were purchased from Sigma. AzaSAM (*21*) and azaMeSAM (*22*) were provided by M. Thompson and M. Blackburn (University of Sheffield), and the anti-SAH MAb (*23*) was a gift from F. Frantzen (Axis-Shield plc/Abbot International, U.K.). SAH hydrolase was obtained as part of a diagnostic kit from Axis-Shield plc. HiTrap NHS-activated Sepharose columns, Sephadex G-50, and Nick Spin columns were purchased from Pharmacia Biotech, T7 RNA polymerase in vitro transcription kits were from Ambion Inc. (MEGAShortscript) or Promega (RiboMAX), and RT-PCR kits were from Promega or Gibco BRL. Centriflex spin columns and QuickPrecip were from AGTC. Sensor chips CM5, HBS buffer, and amine coupling reagents were obtained from Biacore AB, and isotopes and sequencing reagents were from Amersham International. Plasmid miniprep, PCR purification, and gel extraction kits were from Qiagen, and the Zero Blunt PCR cloning kit and TOP10 One Shot competent cells were from Invitrogen. Deep Vent polymerase and T4 polynucleotide kinase were purchased from New England Biolabs, and Nusieve GTG agarose was from FMC. All buffers and solutions were made with diethyl pyrocarbonate-(DEPC) treated (0.1%) and autoclaved water.

Library Construction and RNA Pools. The library template was a 107-mer synthetic DNA oligonucleotide (5′-CGAATTCAGGACTCCTGACATATG(N_{60})GTCATCAGTGCGCAGGATCCATC-3′), containing 60 randomized positions and constant 5′ and 3′ flanking regions for primer-binding and restriction enzyme recognition sites. The ssDNA library was size-purified on 12% polyacrylamide/8 M urea gels and amplified by 8−10 cycles of PCR, using DeepVent DNA polymerase and primers EB1 (5′-TAATACGACTCACTATAGGGCGAATTCAGGACTCCTG-3′ (T7 promoter underlined) and EB2 (5′-GATGGATCCTGCGCACTG-3′). The complexity of the dsDNA library was estimated at 2×10^{14} variants, after correction for a frequency of 30−40% nonamplifiable sequences. The purified PCR products (127 bp) were used as templates for large scale T7 RNA polymerase in vitro transcription reactions with [α-^{32}P]GTP as radioactive tracer. The RNA pool was digested with DNase, phenol-extracted, purified on Sephadex G-50 columns, ethanol-precipitated, and dissolved in DEPC-treated water.

In Vitro Selections: SAH was coupled by its α-amino group to 1 mL of HiTrap NHS-activated Sepharose columns according to the manufacturers instructions. Prior to the first and second selection cycle, the RNA pool was counterselected on columns blocked with ethanolamine to remove matrix- or linker-binding variants. In the first cycle, 7 nmol of [α^{32}P]GTP RNA in RNA buffer (300 mM NaCl, 25 mM Tris, pH 7.6, and 5 mM $MgCl_2$) was loaded on the column, whereas 1 nmol was used in subsequent cycles. After 10−12 min of incubation, the column was washed with RNA buffer (10−15 mL) and bound RNAs were affinity-eluted with 3 column volumes of 10 mM SAH (dissolved by brief heating at 50 °C). The eluates were pooled and precipitated with ethanol in the presence of QuickPrecip or glycogen, and the yield of RNA was assessed by Cerenkov counting. The RNA was reverse-transcribed, PCR-amplified, and retranscribed to generate a new ^{32}P-RNA pool for the next round of selection. The number of PCR cycles was gradually decreased as the yield of RNA increased. In the sixth cycle, the column concentration of SAH was reduced from 4 to 1 mM, and 20 mM SAH was used to elute the RNA. For counterselection (cycles 8−13): Bound RNA was first eluted with 3 mL of 20 mM SAM, the column was washed, and remaining RNAs were eluted with 3 mL of 20 mM SAH. Fractions eluted with SAH were precipitated and amplified. For reselection: The sixth-round binding pool was subjected to eight new cycles of affinity selection on columns derivatized with 1 mM SAH. The RNA was eluted with 40 mM DTT, followed by 40 mM DTT/DL-Hcy and CTH (DTT was used to prevent Hcy dimerization). Remaining RNAs were eluted with 20 mM Ado and SAH. Fractions eluted with DTT/DL-Hcy and CTH were pooled and used as input for the next round.

Cloning, Sequencing, and Secondary Structure Predictions. The SAM-eluted RNA from the eight-cycle counterselection was reapplied to the column and eluted in a series with 20 mM Ado, 20 mM SAH, and 20 mM SAM, using 5 mL wash steps in between. Fractions eluted by each agent were precipitated, reverse transcribed, PCR-amplified, and ligated into the pCRBlunt vector. In the thirteenth cycle, the RNA was

eluted with 20 mM SAM, SAH, and CTH and processed as above. Following the eighth-, and thirteenth-round elutions, the columns were incubated with SAH hydrolase for 1 h at 37 °C. The released material was precipitated, amplified, and cloned. Sequencing was performed either manually, with a cycle sequencing kit with ^{33}P-ddNTPs and a pCRBlunt-specific primer (5′-GCGTTAGAATACTCAAGCTATGC-3′), or in an ALF DNA sequencer (Pharmacia Biotech) with fluorescein-labeled M13 forward and reverse primers. The programs RNADraw, version 1.0 (*24*), and Mfold, version 3.0 (*25*), were used for predictions of RNA secondary structure.

Transcription of Individual RNAs. Templates for in vitro transcription were generated by PCR amplification of the cloned inserts, with Deep Vent DNA polymerase and primers EB1 and EB2. Products of the expected size were purified from 3% Nusieve agarose gels, reamplified, and transcribed in vitro by T7 RNA polymerase. The RNA was phenol-extracted, ethanol-precipitated, and separated from remaining nucleotides on Nick Spin columns equilibrated with RNA buffer (with or without 5 mM Mg^{2+}).

Binding Specificity by Affinity Chromatography. [γ^{32}P]-5′-labeled RNA (1−2 pmol) in RNA buffer containing 5 mM Mg^{2+} was denatured for 10 min at 70 °C, slowly cooled to room temperature, and loaded onto HiTrap SAH affinity columns derivatized with ∼4 mM SAH. Following 25 min of incubation, the column was washed with 8 mL of buffer and the bound RNA (approximately 30% of the total RNA applied) was eluted with a concentration series of each analogue (0.01, 0.025, 0.1, 0.5, and 1 mM), using 4 column volumes at each concentration. The amount of RNA in each fraction was quantified by Cerenkov counting and expressed as percentage of the total SAH-bound RNA (100%). After the final elution, the column was treated with high concentrations of SAH (4 mM) to remove remaining RNAs. When required, the analogues were dissolved by heating to 40−50°C for 10−15 min.

Biosensor Analysis. Real-time interaction analysis was performed in a surface plasmon resonance-based Biacore X optical biosensor. The instrument monitors the change in refractive index that occurs at the sensor chip surface when molecules in solution (delivered by continuous flow) bind to the immobilized ligands. The signal is proportional to the mass of the molecules and is measured in resonance units (RU). (a) Immobilization: SAH (0.1−6.25 mM) in carbonate buffer (0.05 M $NaHCO_3$ and 0.125 M NaCl, pH 8.3) was immobilized onto flow cell 2 of sensor chip CM5, by standard amine coupling protocols. The level of immobilized SAH was estimated as the binding capacity of the surface for anti-SAH MAbs. Flow cell 1 was deactivated with ethanolamine and used as reference surface for subtraction of bulk effects and nonspecific binding. (b) Aptamer binding: Chips with a maximum response level of 9−13 kRU for the anti-SAH MAb were used for most experiments. The RNA samples, dissolved in RNA buffer with or without 5 mM Mg^{2+}, were passed through flow cells 1 and 2, usually in a volume of 30 μL and at a flow rate of 2−5 μL/min. The composition of running and sample buffers were matched and the concentrations of Mg^{2+} and Mn^{2+} were adjusted from 1 M stock solutions of $MgCl_2$ and $MnCl_2$. After each binding cycle the chip was regenerated with concentrated solutions of SAH (2−5 mM, 10 μL at a flow rate of 2 μL/min) or alternatively with a pulse of 50 mM NaOH (pH >12) when the concentration of divalent cations were low. The instrument was primed once or twice with running buffer for each change of buffer. (c) Aptamer kinetics: Rate and affinity constants were obtained by global fitting of the response curves from a range of RNA concentrations to the interaction models provided by the Biaevalution 3.0 software. Exceptions were at high concentrations of Mg^{2+} and Mn^{2+}, where only the affinity of aptamer A8-2 at 50 mM Mn^{2+} was examined in detail. Affinity and rate constants for the other aptamers were in these cases estimated from duplicate injections of a single chosen concentration. (d) Affinity in solution: Equilibrium mixtures (overnight incubations of 1 μM CTH-5 with 0.1−2 μM SAH) were injected over a chip with a binding capacity for anti-SAH of 10 kRU. The concentration of free CTH-5 at equilibrium was determined by comparing the slopes of the association curves to those of CTH-5 in the absence of competitor (calibrating injections). Plots of free CTH-5 versus concentration of SAH were fitted to the equation for solution affinity to give the apparent K_d. (e) Anti-SAH MAb: The anti-SAH MAb is used in a diagnostic kit for indirect determination of total Hcy in plasma or serum (*23* and references therein). Measurements with the MAb were performed in HBS buffer (10 mM HEPES, pH 7.4, 150 mM NaCl, 3.4 mM EDTA, and 0.005% P-20). After each binding cycle the chip was regenerated with a pulse of 50 mM NaOH (10 μL, flow rate 20 μL/min). Kinetic experiments were performed on chips with two different levels of immobilized SAH (10 and 4 kRU for the MAb), and with high flow rates (50−75 μL/min) to minimize mass transport effects. Binding was also tested on chips with lower ligand densities (90−1000 RU MAb response).

Binding Specificity by Biosensor Analysis. Aptamer CTH-5 (0.15 μM in RNA buffer containing 20 mM Mg^{2+}) was injected at a flow rate of 2 μL/min over a chip with a binding capacity of 14 kRU for anti-SAH. Five minutes into the dissociation phase the analogues were injected at flow rate of 2 μL/min for 10 min (0.01 mM in RNA buffer with 20 mM Mg^{2+}). After each binding/elution cycle, the chip was regenerated with a concentrated solution of SAH (2−5 mM), followed by washing with buffer for 3 min. The sensorgrams were normalized in the *y*-direction and overlaid. A portion of each dissociation curve was fitted to the Langmuir 1:1 model to estimate dissociation rates.

Construction of a Minimal CTH-5 Aptamer. The 61-mer oligonucleotide (5′- GATAATACGACTCACTATAGGGC**G**-GATGAGACGCTTGGCGTGTGCTGTGGAGAGTCATC-**C**G), containing 39 nts of the CTH-5 sequence and a T7 promoter (underlined), was purified by HPLC and amplified by PCR with primers PCR-1, 5′CGGATGACTCTCCA-CAGCAC, and PCR-2, 5′GATAATACGACTCACTAT-AGG. Two positions in the putative stem region were changed from A·U to G·C (boldface type) to increase the stability of the construct. The PCR products were used as templates for T7 in vitro transcription reactions, and the 42-mer RNA transcripts with three 5′ terminal Gs from the T7 promoter were purified as above.

RESULTS

Selection of SAH-Binding Aptamers. Aptamers for SAH were selected on columns derivatized with 4 mM SAH. The

A)

Library:		-GGGCGAAUUCAGGACUCCUGACAUAUG-	- (N_{60}) -	-GUCAUCAGUGCGCAGGAUCCAUC	
		(27)		(23)	
a) Classic AMP-aptamer motif:					insert (nt)
+ (7)	A8-3	-GGGCGAAUUCAGGACUCCUGAC*	-CCUCUGAUACGUGGAAGAAACUGCGAACUCCUAGUUCGGAC	-GUCAUCAGUGCGCAGGAUCCAUC	41
(1)	HCY-5	-GGGCGAAUUCAGGACUCCUGA*	-UUCCUCUGAUACGUGGAAGAAACUGCGAACUCCUAGUUCGGAG	-GUCAUCAGUGCGCAGGAUCCAUC	43
+ (1)	SAM-1	-GGGCGAAUUCAGGACUCCUGACAUAUG-	AGGGCUGGAAGAAACUGCAUAACGAACCAAUUGGAAUGUCGUUGUGGA	-GUCAUCAGUGCGCAGGAUCCAUC	48
(1)	HYD-2		-ACGUGGAAGAAACUGCGAACUCCUAGUUCGGAC	-GUCAUCAGUGCGCAGGAUCC*	33
b) Motif-2:					
+ (8)	A8-2	-GGGCGAAUUCAGGACUCCUGACAU*	-GUAGUUGAUUGAAGGACGUUUGAUUCUUAUGGAUUGUGGAAAGCUUCG	-GUCAUCAGUGCGCAGGAUCCAUC	48
+ (1)	SAH-4	-GGGCGAAUUCAGGACUCCUGACAUAUG	-AAUCCGGUUGCCGCUGAUUACAUCAUGUGGAGAGCUUGAUACUAUUGAGGAUGCUUGUGAG-	GUCAUCAGUGCGCAGGAUCCAUC	61
+ (2)	CTH-5	-GGGCGAAUUCAGGACUCCUGACAUAUG	-AUGUUUUAUGGUUAUGCUCUGCGAAAUCACUGAUGAGACGCUUGGCGUGUGCUGUGGAGA	-GUCAUCAGUGCGCAGGAUCCAUC	60
+ (2)	SAH-6	-GGGCGAAUUCAGGACUCCUGACAUAUG	-AUAUCCACUCGAUGCUUGGCUGAUGGAGGUGGACUCGUUCCACAGUUGUGGAGAGGUGUG	-GUCAUCAGUGCGCAGGAUCCAUC	60
c) No clear consensus:					
- (1)	SAM8-3	-GGGCGAAUUCAGGACUCCUGACAUAUG	-GUCCAUCCGUCUGACGAAACUUCCAAAGUUUCUAUCUUCGUUGGGAAGUGUAUGGGCUAC	-GUCAUCAGUGCGCAGGAUCCAUC	60
- (1)	SAM8-4	-GGGCGAAUUCAGGACUCCUGAC*	-GUUAGGGUAAUGGCUCUUCCCAGUAAUGGCUCA	-GUCAUCAGUGCGCAGG*	33
- (1)	SAH-1	-GGGCGAAUUCAGGACUCCUGACAUAUG	-UGAGAUACACCCCGCGUAGGCUGUACCAUCCAUCCUCCUGU	-GUCAUCAGUGCGCAGGAUCCAUC	41
- (1)	SAH-7	-GGGCGAAUUCAGGACUCCUGACAUAUG	-AUGUGACUAUAGAUAUCGUAUUCAUACGUGGGGCAGUUCCGGGUAUGUCGUAUACUUGGU	-GUCAUCAGUGCGCAGGAUCCAUC	60
+ (2)	CTH-2	-GGGCGAAUUCAGGACUCCUGACAUAUG	-AUGGUAUGACUUAAUGUGCUCGGUACUGAUAUGUUGCCACUCGCUUUAAGUAGUCUCGUA	-GUCAUCAGUGCGCAGGAUCCAUC	60
+ (1)	SAH-8	-GGGCGAAUUCAGGACUCCUGACAUAUG	-CUGUCCAUCUUGCGCAUAAAAUUCGAGCCAUGGGCUCGGUCACUUGGCGAACAGUGUGAG	-GUCAUCAGUGCGCAGGAUCCAUC	60
d) Short library inserts					
(1)	HYD8-1	-GGGCGAAUUCAGGACUCCUGACAUAUG	-GUU	-GUCAUCAGUGCGCAGGAUCCAUC	3
- (1)	HYD8-3	-GGGCGAAUUCAGGACUCCUGACAUAUG	-UU	-GUCAUCAGUGCGCAGGAUCCAUC	2
- (1)	HYD8-4	-GGGCGAAUUCAGGACUCCUGACAUAUG	-CUAUCGGUUCGGGUCAUC	-GUCAUCAGUGCGCAGGAUCCAUC	18
(1)	HYD8-5	-GGGCGAAUUCAGGACUCCUG*	-UGUCAC	-GUCAUCAGUGCGCAGGAUCCAUC	6
(1)	HYD8-6	-GGGCGAAUUCAGGACUCCUGACAU*	-CU	-GUCAUCAGUGCGCAGGAUCCAUC	2
(1)	HYD8-2	-GGGCGAAUUCAGGACUCCUGACAUAUG	-AU-	-GUCAUCAGUGCGCAGGAUC*	2
(1)	SAM8-2	GGGCGAAUUCAGGACUCCUG*	-UGCUAAA	-GUCAUCAGUGCGCAGGAUCCAUC	7
(1)	CTH-1	-GGGCGAAUUCAGGACUCCUG*	-UUUGGUCAUUU	-GUCAUCAGUGCGCAGGAUCCAUC	11
- (1)	HCY-2	-GGGCGAAUUCAGGACUCCUG*	-UCAUCAGCUCGGCUUGUCAU	-GUCAUCAGUGCGCAGGAUCC*	20
(1)	HCY-4	-GGGCGAAUUCAGGACUCCUGA*	-U	-GUCAUCAGUGCGCAGGAUCCAUC	1
(1)	HYD-1	-GGGCGAAUUCAGGACUCCUGACAUAUG	-GCAAUAUCC	-GUCAUCAGUGCGCAGGAUCCAUC	9
(1)	SAH-9	GGGCGAAUUCAGGACUCCUGACAUAUG	-CGCACA	-GUCAUCAGUGCGCAGGAUCCA*	6
(1)	SAH-10	GGGCGAAUUCAGGACUCCUG*	-UUGUGUG	-GUCAUCAGUGCGCAGGAUCCAUC	7

B)

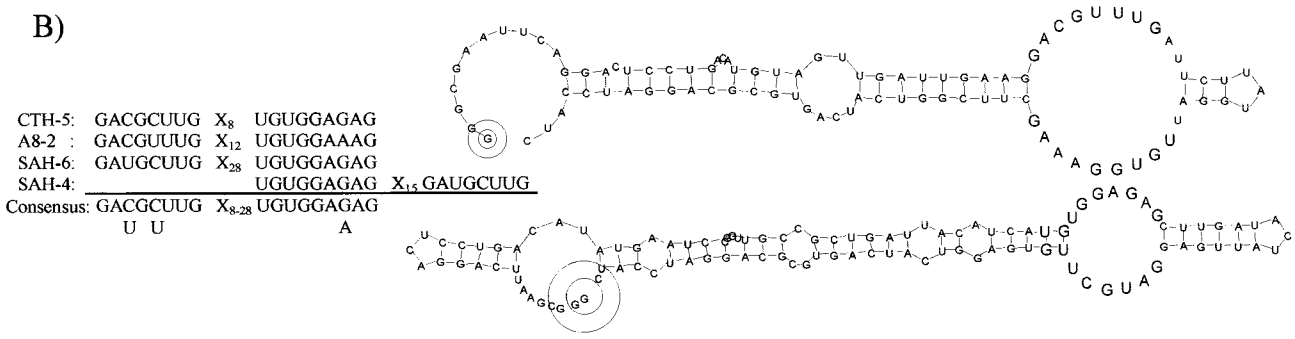

FIGURE 2: Sequences, consensus motifs, and secondary structures. The RNA library with 60 randomized positions is shown at the top. (A) Sequences of aptamers from the eighth and thirteenth selection cycles. The number of identical isolates and the length of the randomized region are indicated in parentheses to the left and to the right of each sequence, respectively. Consensus motifs are underlined. (a) Sequences containing the Ado-binding motif (ATP aptamers). (b) Sequences with the motif 2 consensus. (c) Sequences with no apparent similiarities. (d) Truncated sequences with deletions (*) in the library and left flanking regions. The T7 transcripts of sequences marked + and − were tested for binding to SAH in the biosensor (+, binds SAH; −, no detectable binding).[2] (B) Left: Conserved regions of the Motif-2 aptamers (X = variable nts). Right: Predicted secondary structure for two of the Motif-2 aptamers, A8-2 (top) and SAH-4 (bottom). Conserved nts are enlarged.

starting ^{32}P-pool contained ~10^{14} 110-mer RNA variants, each with a randomized region of 60 nts (the library) and fixed 5′ and 3′ flanking regions. After 7 rounds of selection−amplification, 22% of the applied RNA eluted with SAH. By reasoning that a significant proportion of the RNAs at this stage were likely to represent Ado-recognizing aptamers, counterselection with SAM (that differs from SAH by a methyl group and a positive charge, Figure 1) was introduced from the eighth round on. Counterselection resulted in a large drop in the SAH-eluted fraction that in the following five rounds never exceeded more than about 2%. As this suggested that the Ado moiety of SAH still formed part of the recognition site for a majority of the RNAs, an elution with cystathionine (CTH, a thioether-linked dipeptide of Hcy and serine, Figure 1) was included in the eleventh round. The small but detectable amount of RNA released by CTH was combined with the SAH-eluted fraction and amplified. In the thirteenth and final round, RNAs from serial elutions with SAM, SAH, CTH, DL-Hcy, and Ado were reverse-transcribed, PCR-amplified, and cloned into the pCR-Blunt vector for sequencing. Some of the remaining (nonelutable) RNAs on the column were recovered by treatment with the enzyme SAH hydrolase. The enzyme cleaves the thioether bond between Hcy and Ado and presumably releases the Ado moiety of SAH and any high-affinity RNA bound to it. Significant amounts of radiolabeled material were indeed released, but it is unclear to what extent the change in buffer and temperature conditions (pH 8.1, no Mg^{2+}, 37 °C) might have contributed to the effect.

Sequence Analysis. Sequencing of 43 clones from the eighth- and thirteenth-round binding pools revealed two dominant sequence families; the ATP (Ado-recognizing) aptamers identified previously (*11*) (23%) and a novel class (motif 2, 30%) containing two short conserved regions of 8 and 9 nts (Figure 2). The conserved regions were spaced by a variable number of nts (8−28) and in one case they appeared in reversed order (SAH-4, Figure 2B). The most abundant variant of the motif 2 class (A8-2; eight isolates) was present among

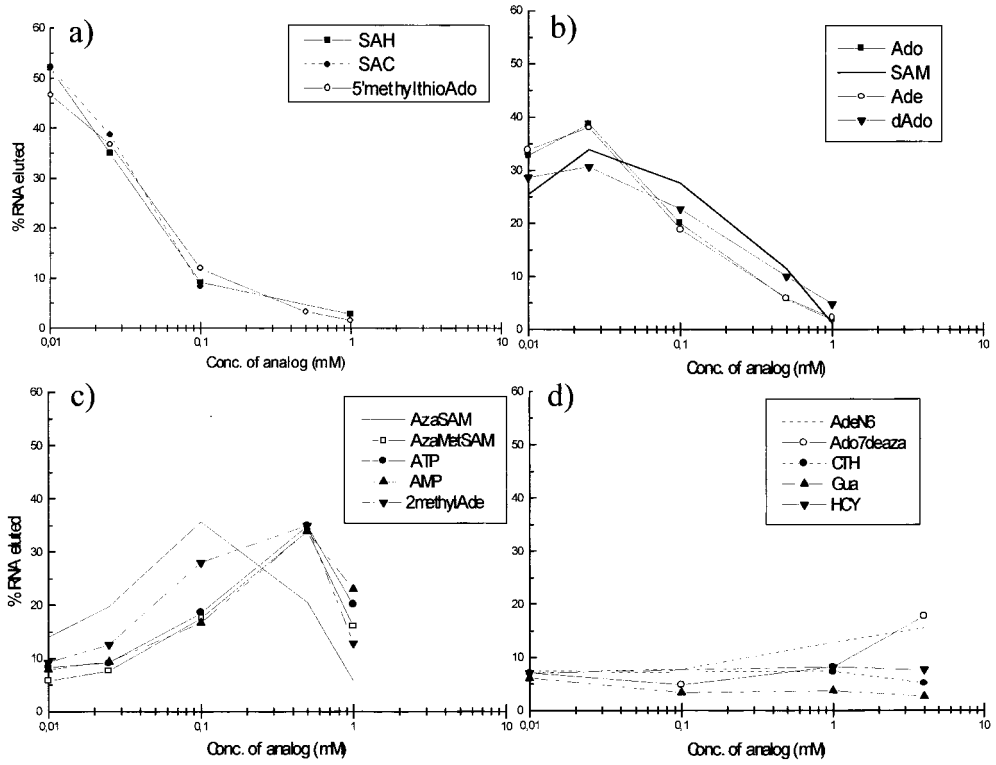

FIGURE 3: Binding specificity; competitive elution of ^{32}P-CTH-5 RNA from SAH columns by SAH-related molecules. The elution profile of each analogue in the concentration range 0.01−1 mM is shown. The analogues were applied in a consecutive series of increasing concentrations. Each data point represents the amount of RNA eluted by 4 column volumes of analogue at the indicated concentration, expressed as percentage of the total bound RNA (100%). The analogues were grouped into four categories (I−IV, panels a−d) on the basis of their ability to compete with immobilized SAH. The analogues in panel d were also tested at 4 mM. The values are averages of at least two independent experiments.

the eight- round sequences, whereas the other three (CTH-5, SAH-4, and SAH-6) appeared in the final round. A third group of sequences showed no obvious similarities except for short matches of 5−6 nts. Surprisingly, all but one of the sequences from SAH hydrolase treatment of the column proved to contain very short library regions (1−20 nts instead of the original 60). However, as there was no obvious pattern for the deletions, and RNA from these sequences did not bind to SAH, their origin remains unexplained. Deletions of the library- and left flanking regions had also occurred for the ATP aptamers and for aptamer A8-2 (41−48 nt randomized regions remaining). A reselection of the sixth-round binding pool, with more direct selection for aptamers by affinity for the Hcy moiety of SAH (elution with Hcy and CTH), did not result in significant enrichment. Only two types of sequences were recovered after eight additional selection rounds; the ATP aptamer and A8-2 from the motif 2 class (14 clones sequenced).

The proposed secondary structures of two of the motif 2 aptamers are shown in Figure 2B. With the exception of SAH-6 (with very long spacing between the conserved elements), the folding of the motif 2 aptamers was similar, and alternative structures with slightly higher energies mostly affected the size of the internal loop. The presence of the two conserved elements on opposing sides of the predicted internal loop (and in both orientations) clearly indicates an important role for these nts, which was further supported by the functional properties of a 39-mer minimal CTH-5 construct containing this region (Figure 10).

Binding Specificity: (a) Interactions with the Hoogsteen Face of Adenine and the 5′ Substitutent. Positions on SAH involved in binding to the motif 2 aptamer CTH-5 were defined by competitive elution with 16 different SAH, SAM, Ado, and adenine analogues. The analogues were applied to the column in a five-step concentration series, starting with 0.01 mM, the minimal concentration of SAH required to elute about 50% of the bound RNA in 4 column volumes. The concentration of analogue required to elute the majority of RNA was used as a measure of competition efficiency. The analogues could be grouped into four categories on the basis of their ability to compete with immobilized SAH (Figure 3, panels a−d, respectively). Compounds with truncations of the Hcy side chain (*S*-adenosylcysteine and 5′-thiodeoxymethyladenosine, group I) competed as well as SAH, suggesting that the region 5′ to the thioether region is not required for binding. The group II compounds (SAM, Ado, 2′-dAdo, and adenine) were required at 2.5-fold higher concentrations to elute the majority of RNA, indicating predominant recognition of adenine and the presence of another (minor) contact point at the 5′-end of the ribose. This contact point could be either lacking (for Ado and adenine) or sterically or electrostatically preventing in the case of SAM. Constraints on the 5′-environment were also indicated by poor elution efficiencies of ATP and AMP (group III), which were 50-fold lower than for group I. Group IV contained compounds that failed to elute or eluted very

[2] Note: Sequencing revealed that four of the plasmids (SAH-4, SAH-8, CTH-2, and HYD8−4) contained double inserts. The additional sequences were either truncated sequences with 1−2 nt randomized regions or sequences shown to be inactive or weak-binding as RNAs.

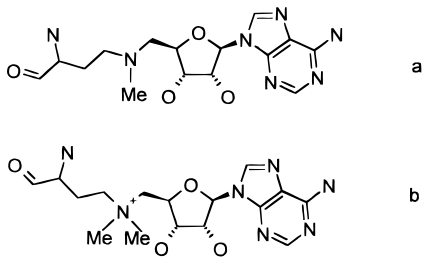

FIGURE 4: Structures of (a) azaSAM and (b) azaMeSAM. The predominant form of AzaSAM at pH 7.6 is shown ($pK_a = 7.1$, *21*).

poorly even when tested at high (4 mM) concentrations (guanosine, DL-Hcy, and CTH). Lack of binding to guanosine confirms specificity for adenine, whereas lack of binding to CTH shows that the thioether region is by itself insufficient for recognition. Derivatives of adenine with substitutions at position N6 and N7 also failed to elute the RNA, whereas modification at position C2 had less severe effects. Thus, the Hoogsteen face (N6 and N7) of the adenine base appears to provides the most important contacts with the aptamer, whereas a secondary interaction site at the 5′position of the ribose confers the observed preference for SAH.

(b) Recognition of the Sulfur/Thioether Region of Hcy. To probe the basis for SAH specificity in more detail, and in particular the role of the sulfur atom, the ability of two azaSAM derivatives (Figure 4) to compete with SAH was assessed. In addition to the sulfur to nitrogen change, AzaMeSAM (*22*) carries an extra methyl group and has a higher positive charge density than SAM. AzaSAM (*21*) is isosteric with SAM but is largely uncharged (>70%) at the assay conditions of pH 7.6 and in this respect more similar to SAH. The following reasoning was applied: if either the charge or the methyl group of SAM is responsible for reduced competition (Figure 3b) *and* the nitrogen−sulfur change is not important; then azaSAM is expected to compete either better (because it is largely uncharged) or the same as SAM (because they both have a single methyl group). As shown in Figure 3c, however, both analogues competed significantly less effectively than SAM (4× and 20×, respectively). The fact that azaSAM was 4-fold less effective than SAM (and 10-fold less effective than SAH) indicates that the sulfur or the thioether environment may play a role in specific recognition of SAH. The fact that the methylated derivative was 5-fold less effective than azaSAM (or 50-fold less than SAH) suggests that the extra methyl group sterically interferes with binding to the extent that contacts with the major interaction site on adenine are also prevented. Furthermore, the almost identical elution profiles of azaMeSAM and ATP/AMP suggest that these compounds prevent aptamer binding by similar mechanisms.

(c) Binding Specificity by Biosensor Analysis. In the course of biosensor analysis it was observed that the chip could be effectively regenerated by high (millimolar) concentrations of SAH, most likely due to competition between injected and immobilized SAH for the RNA. The extent of regeneration could easily be manipulated by varying the concentration of SAH and/or the time of exposure. By measuring the relative abilities of SAH analogues or other compounds to "elute" the RNA from the chip, the binding specificities of the aptamers could be determined. Figure 5a shows the results for aptamer CTH-5, using the analogues in group I and II (Figure 3a,b) as competitors injected during the dissociation phase. As for the column experiments, a concentration of 0.01 mM analogue was required to achieve discrimination between these closely related compounds. With the possible exception of *S*-adenosylcysteine (SAC), which in this assay competed even better than SAH (the side chain of SAC is one carbon unit shorter than for SAH), the ranking of analogues was the same as determined by the column experiments. The difference in Mg^{2+} concentration (20 mM versus 5 mM for the column experiments) did not seem to affect specificity. Comparisons of dissociation rates in the presence and absence of competitor showed that aptamer CTH-5 discriminates between SAH and other adenine-containing compounds tested in this experiment by no more than a factor of 2−3 (Figure 5b). As previously shown, however, discrimination was higher toward other adenine-containing compounds such as ATP or azaSAM, which were required at much higher concentrations than 0.01

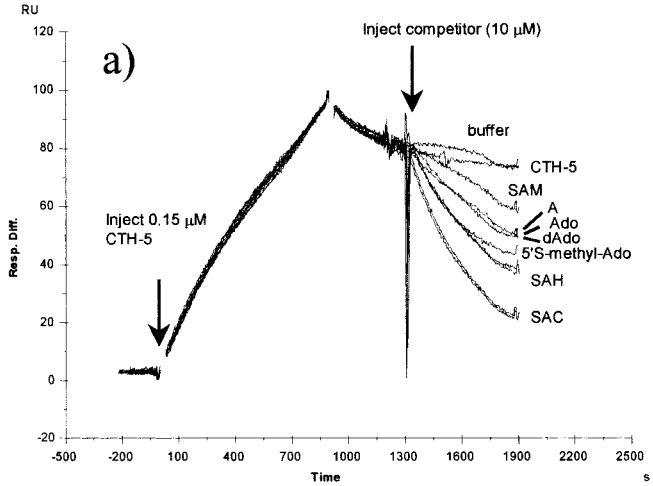

b)

Competitor	k_d (s^{-1})	k_d SAH/ k_d competitor
-	$1{,}4 \times 10^{-4}$	-
buffer	$1{,}3 \times 10^{-4}$	-
SAM	$5{,}1 \times 10^{-4}$	2,9
Ade	$7{,}4 \times 10^{-4}$	2,0
Ado	$9{,}4 \times 10^{-4}$	1,6
dAdo	$9{,}6 \times 10^{-4}$	1,5
5'S-Ado	$1{,}3 \times 10^{-3}$	1,1
SAH	$1{,}5 \times 10^{-3}$	1.0
SAC	$2{,}4 \times 10^{-3}$	0,6

FIGURE 5: Binding specificity in the biosensor. (a) Aptamer CTH-5 (0.15 μM) was injected at a flow rate of 2 μL/min in the presence of 20 mM Mg^{2+}. The analogues (0.01 mM) were injected 5 min into the dissociation phase (arrow). The curves were normalized in the *y*-direction and overlaid. (b) Dissociation rates (k_ds) in the presence and absence of competitor, estimated from fitting of a portion of the dissociation curves to the 1:1 interaction model. The ratio of the k_d in the presence of SAH to k_d in the presence of competitor gives apparent discrimination factors. dAdo = 2′-deoxyadenosine; 5′-SMeAdo = 5′-thiodeoxymethyladenosine.

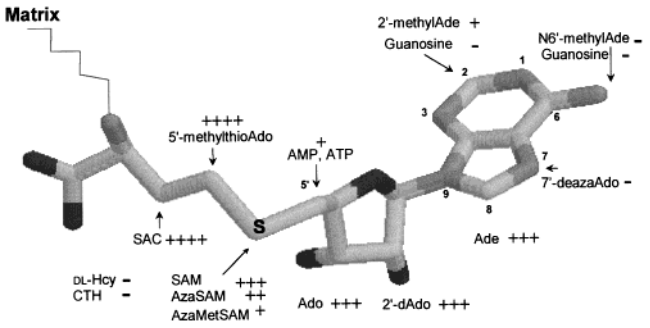

FIGURE 6: Summary of competition experiments. The ability of each analogue to compete with immobilized SAH is indicated by + and − signs (++++, competes as well as SAH).

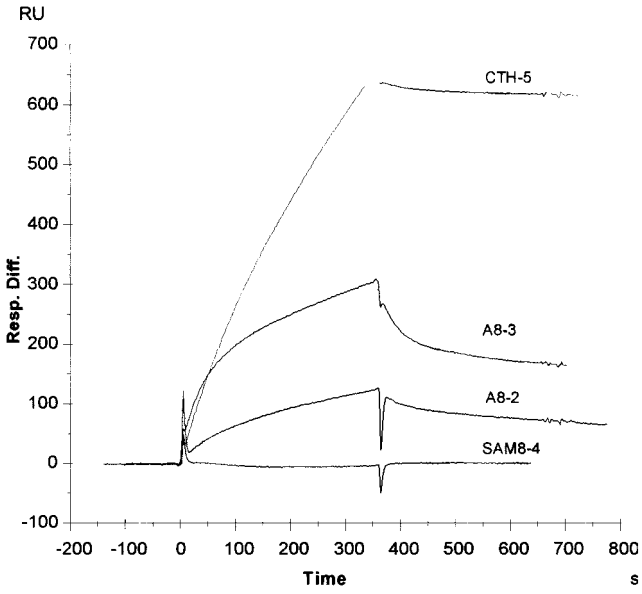

FIGURE 7: Kinetic ranking at selection conditions (5 mM Mg^2). Binding of four representative aptamers to immobilized SAH (CTH-5 and A8-2 from the motif 2 class, A8-3 from the ATP class, and the nonbinding SAM8-4 from the no clear consensus class). The aptamers (4.2 μM) were injected over the SAH chip at a flow rate of 5 μL/min. The binding response reflect differences in binding rates as well as differences in molecular weight (the response observed is directly proportional to mass). A8-2, 31 kDa; A8-3, 28 kDa; CTH-5, 35 kDa; SAM8-4, 23 kDa.

mM to elute the RNA from the chip (Figure 3c). The binding specificity results are summarized in Figure 6.

Kinetic and Affinity Analysis: (a) Kinetic Profiles. The kinetics of the aptamer−SAH interaction were studied in a Biacore X biosensor, initially at in vitro selection conditions (5 mM Mg^{2+}) and with SAH immobilized onto the chip. Of 15 aptamers tested, eight gave detectable signals and bound to varying extents (all four motif 2 aptamers, two variants of the ATP aptamer class with different flanking regions, and SAH-8 and CTH-2 from the no clear consensus class). A comparative ranking is shown in Figure 7. The most stable binding (slow dissociation) was shown by the motif 2 aptamers SAH-4 and CTH-5. The ATP aptamers, apparently in the same affinity range as the SAH aptamers, showed slightly faster dissociation rates and more pronounced biphasic binding curves. The most obvious characteristic of all aptamers, however, was a very slow rate of association, with the consequence that equilibrium binding or steady-state levels could not be reached during the time available for injection (maximum 100 min). From this it follows that

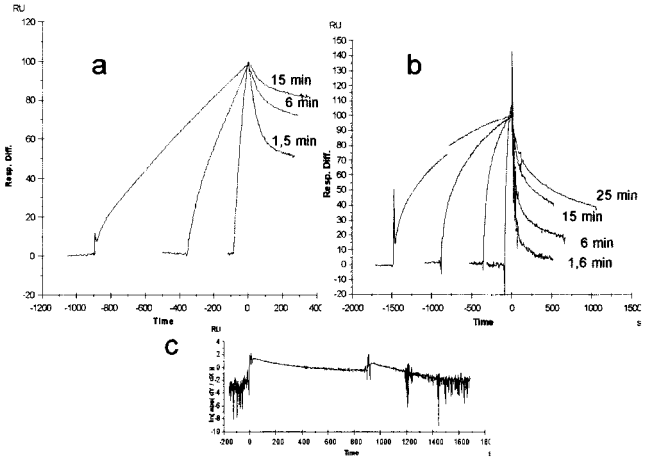

FIGURE 8: Effects of contact time on complex stability (dissociation rates). The aptamers were injected over the SAH chip for variable periods of time (1.5−20 min). The curves were normalized in the *y*-direction and overlaid. (a) Aptamer SAH-4, 1 μM, b) Aptamer A8-2, 4 μM. c) Plot of ln [abs(d*y*/d*x*)] for one of the A8-2 binding curves.

dissociation constants (K_ds) have to be derived from the ratio of the kinetic rate constants (k_d/k_a) or from competition experiments with free SAH to give the affinity in solution. Slow association also made it necessary to use low flow rates (2−5 μL/min) and high levels of immobilized ligand to achieve reasonable binding levels.

(b) Heterogeneous Reaction Kinetics. Analysis of the binding data revealed clear deviations from standard 1:1 reaction kinetics, as evidenced by poor fits to the Langmuir reaction model, nonlinear (concave) derivatized plots (Figure 8c), and increased stability of the complex with longer association times (Figure 8a,b). Common sources for deviation from the 1:1 model, such as nonspecific binding, bulk effects, mass transport limitations, and baseline drift (*26*, *27*) could all be eliminated (not shown). Increased stability with time indicate the existence of two (or more) contributing reactions, which are linked and not independent (*26*). This leaves two alternative reaction models: a two-stage reaction with conformational change or competitive binding by different forms of RNA. These alternatives were not further resolved.

(c) Rate constants and K_ds. As a reasonable approximation, the rate constants for the first and most dominant reaction (which were consistent for all models tested) were used to estimate affinities. Thus, for the aptamers that gave significant binding under selection conditons, the k_a values (on rates) ranged from 10^2 to 10^3 M^{-1} s^{-1} and the k_d values (off rates) from 10^{-4} to 10^{-3} s^{-1}, giving apparent K_ds in the 0.1−10 μM range. The highest affinities were shown by the motif 2 aptamers CTH-5 and SAH-4, with K_ds in the submicromolar range (0.2−0.8 μM). As the contribution of the secondary reaction to affinity was difficult to assess, the values above should be considered as conservative estimates. To avoid the question of reaction mechanism, the affinity of the strongest binding aptamer (CTH-5) for SAH in solution was determined by a competition approach in the biosensor. The apparent K_d of ∼0.15 μM agrees well with the value obtained from kinetics.

Ion Dependency of Binding. In the course of biosensor analysis it was observed that some of the aptamers were highly sensitive to changes in the concentration of Mg^{2+} and

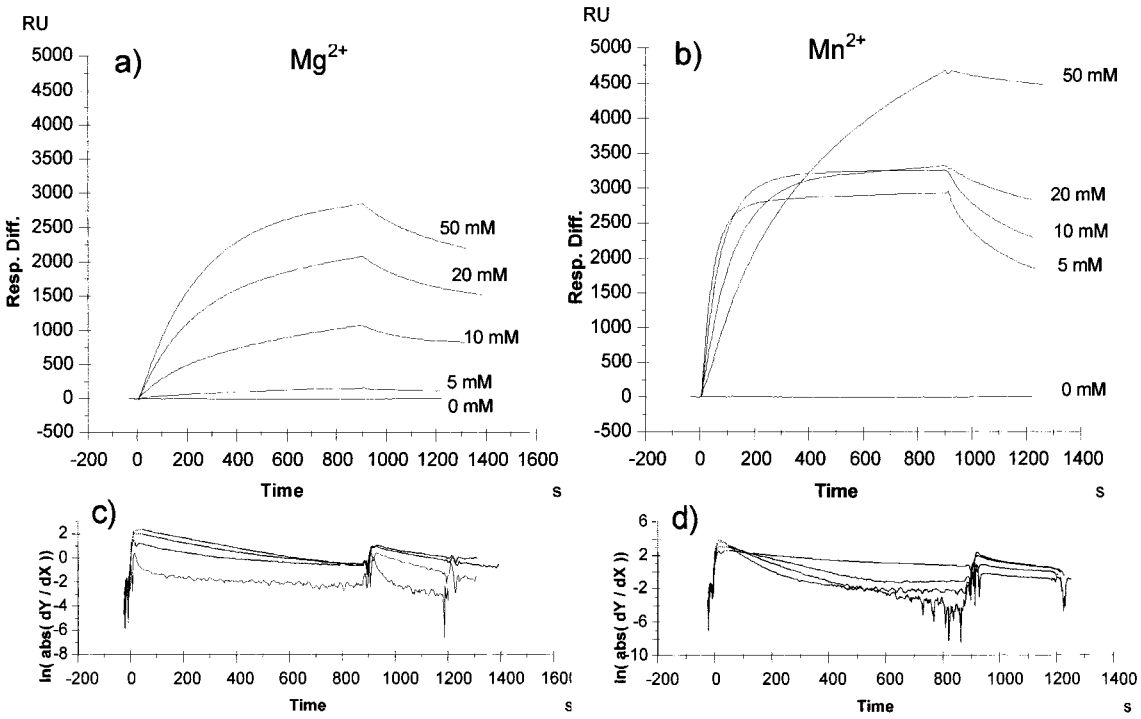

FIGURE 9: Binding of A8-2 at varying concentrations of Mg^{2+} and Mn^{2+}. Aptamer A8-2 (2.5 μM) was injected over the SAH-chip at a flow rate of 2 μL/min for 15 min. (a) Binding in the presence of (a) 0−50 mM Mg^{2+} and (b) 0−50 mM Mn^{2+}. (c, d) Plots of ln[abs(d*y*/d*x*)] for the curves in panels a and b, except those obtained in the absence of divalent cations. The binding capacity of the chip for anti-SAH was 14 kRU.

that this sensitivity also varied between individual aptamers with the same consensus motif. Probably, this is one of the reasons why consistent binding data were sometimes difficult to obtain and that small variations between different batches of buffers could be observed. A systematic survey of the Mg^{2+} and Mn^{2+} dependency of the interaction revealed a remarkable influence of these ions on the kinetic properties of the aptamers. The strongest effects were found for aptamer A8-2 (Figure 9), which showed an absolute requirement for Mg^{2+} or Mn^{2+}, and for which increasing the Mg^{2+} concentration from 5 to 50 mM gave a ~30-fold increase in binding response (Figure 9a). Mn^{2+} proved to be even more effective, giving faster association and higher response levels than at the corresponding concentrations of Mg^{2+} (Figure 9b). Interestingly, at Mn^{2+} concentrations between 20 and 50 mM, the entire kinetic profile of A8-2 changed into that typical for Mg^{2+}. Also, an interesting trend toward less heterogeneous reaction kinetics (more linearity) could be observed from plots of ln d*R*/d*t* with increasing concentrations of ions (Figure 9c,d). When analyzed by a 1:1 interaction model, which was considered appropriate at this concentration of Mn^{2+} (50 mM), the K_d of A8-2 for SAH was estimated at 50−100 nM.

The effects of Mg^{2+} and Mn^{2+} on the binding activity of the aptamers were highly individual and not predictable from sequence alone. For most of the aptamers, 50 mM Mn^{2+} gave the most efficient binding, but for, e.g., aptamer CTH-5 (the strongest binding aptamer at selection conditions), Mg^{2+} was more effective (Figure 10c), although the magnitude of the effect was much lower than for A8-2 (2−3-fold increase). The ATP aptamer (A8-3) showed the expected 3−4-fold increase in response from 5 to 20 mM Mg^{2+} (*11*), and higher concentrations of Mg^{2+} or Mn^{2+} did not enhance binding further (up to 50 mM tested).

Aptamer A8-2, which was the most sensitive to changes in the concentration of Mn^{2+}, actually contains within its predicted single-stranded loop the sequence requirements for forming a 7 nt Mn^{2+}-binding structure (Figure 2B) (*28*). The Mn^{2+}-binding (and self-cleaving) motif consists of a complex between UUU and GAAA, which can form in cis or in trans (*29*) and where specific cleavage is reported to occur between G and A (*28*). Preliminary tests of a putative self-cleaving activity for A8-2, however, revealed that only about 2% of the RNA was cleaved, and that into multiple fragments. Thus, a self-cleaving activity for this sequence motif in A8-2 seems unlikely.

A Minimal CTH-5 Construct Shows Different Kinetic Properties and Ion Dependency. A 39 nt truncated CTH-5 aptamer, containing the predicted internal loop and a short stem region with minor modifications to increase stability, showed kinetic properties that were quite different from those of the parental CTH-5 RNA (Figure 10). The on and off rates were both much faster, and the effects of Mg^{2+} and Mn^{2+} were stronger. However, since k_a and k_d were both higher, the estimated K_d (k_d/k_a) was similar to that of the full-length CTH-5. The results suggest that the 39-mer construct contains the essential elements for binding to SAH, although the change in kinetic profile indicates that flanking regions may also modulate the activity of the aptamers.

Comparison with Anti-SAH Antibody. The availability of an anti-SAH MAb with similar or identical binding specificity as aptamer CTH-5 (Ado/thioether region of SAH; *23*) provides a unique opportunity to compare the kinetics and affinities of two such different recognition entities. Aptamer A8-2, which under conditions of 50 mM Mn^{2+} gave the highest response of the aptamers tested, was chosen for comparison with the MAb. As shown in Figure 11, the most

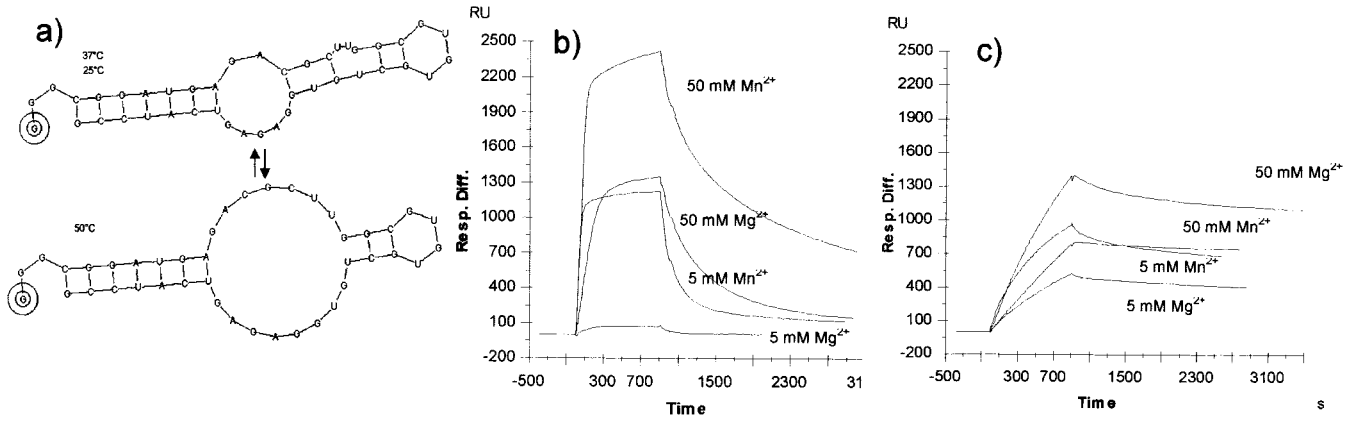

FIGURE 10: Binding of minimal and full-length CTH-5. (a) Sequence and predicted secondary structure of the minimal CTH-5 construct. The construct contains 39 nts from the CTH-5 sequence and three 5′-terminal Gs from the T7 promoter. The second base-pair in the 5′-stem region was changed from A•U to G•C. (b) Binding of truncated CTH-5 (13.4 kDa) to immobilized SAH at varying concentrations of Mg^{2+} and Mn^{2+}. (c) Binding of full-length CTH-5 (35.2 kDa). The concentration of RNA was 1 μM, the flow rate was 2 μL/min, and the binding capacity of the chip for anti-SAH was 10 kRU.

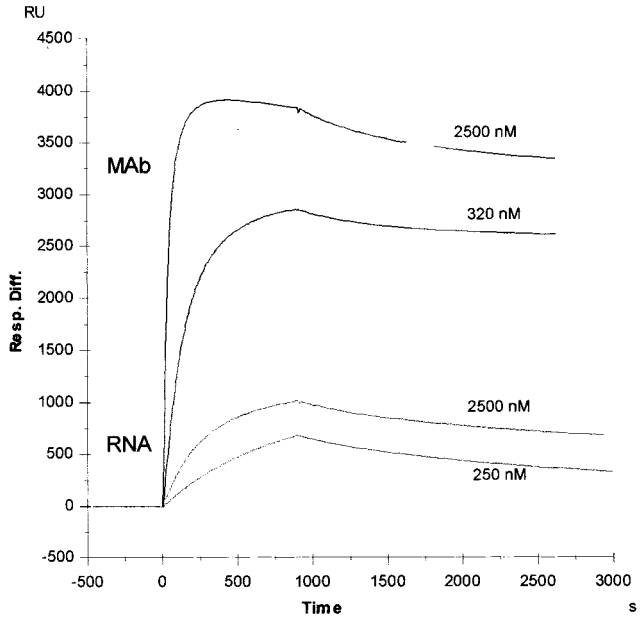

FIGURE 11: Aptamer/MAb comparison. Anti-SAH MAb and aptamer A8-2 were injected at flow rate of 2 μL/min on a chip giving 4 kRU for the MAb. A8-2 was assayed in the presence of 50 mM Mn^{2+} and the MAb in HBS buffer. The response is proportional to mass (31 and 155 kDa for A8-2 and anti-SAH, respectively).

obvious difference between the MAb and the aptamer was the rate of association, which was much faster for the MAb (approximately 10×). Fitting of the response curves from a series of MAb concentrations to the 1:1 Langmuir model gave the following approximate values for the rate constants: a k_a of 1×10^5 M^{-1} s^{-1} and a k_d of 3×10^{-4} s^{-1} (although avidity effects might be involved, the 1:1 model was considered adequate for the purpose inasmuch as fitting to the bivalent analyte model did not improve the fit significantly). From the ratio k_d/k_a, the K_d of the MAb for immobilized SAH was estimated at 3 nM. The corresponding values for aptamer A8-2 were a K_d of 50−100 nM, a k_a of $(3-4) \times 10^3$ M^{-1} s^{-1}, and a k_d of $(2-3) \times 10^{-4}$ s^{-1}. Thus, the difference in affinity between A8-2 and anti-SAH is in the ∼20-fold range.

DISCUSSION

The SAH-binding aptamers characterized in this study provide several new and interesting features. First, the selection identified a novel adenine/Ado-recognizing RNA motif, the third reported so far (*11*, *12*). The novelty of the motif may at least be partly explained by the fact that the adenine moiety of SAH was left free and intact during selection, inasmuch as SAH was attached by its Hcy amino group and not by the adenine C8 (*11*, *14*) or N6 (*12*) positions as in previous cases. Stringent counterselection with SAM may also have contributed to the effect, although it did not prevent the "classic" ATP aptamer from emerging. Another contributing factor may have been the time of exposure to the target, which was long because of counterselection and which could have favored selection of aptamers with slower dissociation rates.

Competition experiments suggested that the affinity of aptamer CTH-5 for Ado/adenine is in the same range (or somewhat better) than previously reported for the adenine- (CoA-) and Ado-recognizing aptamers (0.5 and 0.7 μM at optimized conditions, respectively; *12*, *11*). As for the CoA aptamer, the Hoogsteen face of adenine appears to provide the most important contacts, and binding in the absence of Mg^{2+} was negligible (*12*). In contrast, the ATP aptamer interacts with the Watson−Crick face of adenine and binding is independent of Mg^{2+} (*11*). The Mg^{2+} independence of the ATP aptamers may explain why this motif appears to be the most readily selectable under a variety of experimental conditions (*14*). Remarkably, the ATP aptamers emerging in our selection appeared as "premade" short forms of 41 nts, highly similar in size to the 40-mer minimal aptamer constructed by Sassanfar and Szostak (*11*).

The SAH aptamers are also the first of the Ado/adenine-recognizing aptamers that include a contact with the 5′ substitutent. Although the 5′ sulfur/thioether interaction was by itself insufficient for recognition, it increased the affinity for SAH versus Ado/adenine by a factor of 2−3. However, the fact that presence of bulky/charged 5′ substituents reduced binding up to 50-fold, and bulkiness apparently somewhat more than charge, suggests that there are constraints on the 5′ environment that could be predominantly steric. This again implies that the two binding specificities of the aptamers are

physically close. Considering that only one face of the predicted internal loop contains the typical purine bias of small-molecule aptamer binding sites (*31*), it is tempting to suggest that the two binding specificities of the SAH aptamers may be contributed by regions on either side of the internal loop.

Another interesting feature of the SAH aptamers was an unusual level of ion dependency, where high concentrations of Mg^{2+}, and in particular Mn^{2+}, in some cases increased the maximum response more than 30-fold. The effect of Mg^{2+} on the affinity of aptamers for small ligands appears to be highly variable: e.g., the ATP and CoA aptamers bind their targets with 2−4-fold higher affinities at 20−30 mM Mg^{2+} than at 5 mM Mg^{2+} (*11*, *12*); binding of the citrulline aptamer is prevented at 20 mM Mg^{2+} (*18*); and the theophylline aptamer is unaffected by Mg^{2+} concentrations ranging from 5 to 100 mM (*4*). The SAH aptamers were extremely sensitive to small variations in ion conditions and sometimes collapsed at very high concentrations of Mg^{2+} and Mn^{2+}, even before the injection was finished. Biosensor analysis also revealed that high concentrations of ions mostly affected the rates of association and that each aptamer responded differently to both the type and concentration of ion.

Although the structural properties of the aptamers were not investigated in detail, it seems likely that the effect of ions somehow relates to changes in RNA conformation (see, e.g., ref *31*). Indications of conformational heterogeneity were indeed observed; e.g., most of the RNAs migrated as multiple bands on native gels but not on denaturing gels, and only about 30% of the CTH-5 RNA were in a state able to bind to the SAH affinity matrix, at least when the concentration of Mg^{2+} was low (5 mM). It is possible that elevated concentrations of Mg^{2+} and Mn^{2+} may act to increase the number of active aptamers by stabilizing one of several alternative conformations. Alternatively (or in addition), the affinity of each individual aptamer may be increased by stabilization of the region surrounding the ligand binding site. In the absence of structural data, however, these possibilities cannot be further assessed**.**

In view of the recent coselection of a Mn^{2+}-binding motif in an aptamer originally selected for ligase activity (*32*), the presence of this sequence in the Mn^{2+}-sensitive aptamer A8-2 (and in the assumed ligand-binding site) was intriguing. In neither case was Mn^{2+} present during in vitro selection, suggesting that sequences adapted to Mg^{2+} may easily switch to Mn^{2+} without loss of activity or specificity (*32*). Although the self-cleaning activity of the Mn motif (*28*, *29*, *32*), was not found for A8-2, it cannot be excluded that this particular sequence could play a more subtle role and perhaps be more prone than others to attract ions and thus to increase their local concentration.

The biosensor experiments raised the question of interaction mechanisms and suggested that either a two-state reaction with conformational change or a heterogeneous analyte (competitive) model with two or more competing conformations of RNA best described the data. Although the reaction was clearly heterogeneous, the exact binding mechanism was difficult to determine due to the added complexity of strong ion sensitivity. We note, however, that most aptamers recognizing low-molecular weight ligands interact by a two-state reaction mechanism (adaptive binding), where an initially unstructured RNA undergoes a conformational change upon binding of ligand (*33*).

Mapping of binding specificities in the biosensor proved to be an efficient alternative to the more traditional column-binding studies, giving essentially the same results and avoiding the use of radioactive labels. The assay was used at several levels of precision: in preliminary screens to provide simple yes/no data (with high concentrations of analogues), for semiquantitative ranking and estimation of discrimination factors (starting with a low concentration and increasing until an effect was seen), and for fine mapping of binding specificities (with a concentration of analogue corresponding to the concentration of SAH that eluted approximately 70% of the RNA). Obviously, the method requires that the binding complex is reasonably stable (slow dissociation).

Comparisons with the anti-SAH MAb suggested that the on rate is the limiting factor for high affinity binding by the aptamers. Combined with the fact that increased concentrations of Mg^{2+} and Mn^{2+} mostly affected the rates of association, these findings could be of special interest with regard to the use of aptamers as diagnostic devices (*6*). It may also give clues as to why the affinities of MAbs for small molecules are typically higher (nanomolar; *34*) than what has been found for most aptamers (submicromolar; *1*) characterized to date. Although the kinetic properties of most aptamers have been neither characterized nor tested at high concentrations of ions, it will be interesting to see whether slow association is a general characteristic of small-molecule recognizing aptamers and whether (and to what extent) changes in ion conditions might improve it. It is also interesting to note that the binding specificity of the aptamers was practically identical to that determined for the anti-SAH MAb (*23*), suggesting that the interaction chemistries are overall similar.

ACKNOWLEDGMENT

We are grateful to Mark Thompson and Mike Blackburn (University of Sheffield) for generously providing the azaSAM and azaMeSAM analogues. Mark Thompson is also acknowledged for giving his expert opinion on the chemical properties of the analogues. We thank Erling Sunderhagen, Frank Frantzen, and Ingrid Alfheim (Axis-Shield plc) for initial discussions and for supplying the anti-SAH MAb and SAH hydrolase. Robert Karlsson (Biacore AB) is acknowledged for initial assistance with Biacore analysis and for reading of the manuscript. Finally, we thank Mike Yarus (University of Colorado) for constructive comments.

REFERENCES

1. Gold, L. (1995) *J. Biol. Chem. 270*, 13581−13584.
2. Famulok, M. (1999) *Curr. Opin. Struct. Biol. 9*, 324−329.
3. Tuerk, C., and Gold, L. (1990) *Science 249*, 505−510.
4. Jenison, R. D., Gill, S. C., Pardi, A., and Polisky, B. (1994) *Science 263*, 1425−1429.
5. Wang, Y., Killian, J., Hamasaki, K., and Rando, R. R. (1996) *Biochemistry 35*, 12338−12346.
6. Jayasena, S. D. (1999) *Clin. Chem. 45*, 1628−1650.
7. Finkelstein, J. D. (1990) *J. Nutr. Biochem. 1*, 228−237.
8. Ueland, P. M. (1982) *Pharmacol. Rev. 34*, 223−253.
9. Finkelstein, J. D. (1998) *Eur. J. Pediatr. 157* (Suppl. 2), S40−S-44.

10. Nygard, O., Vollset, S. E., Refsum, H., Brattstrom, L., and Ueland, P. M. (1999) *J. Intern. Med. 246*, 425−54.
11. Sassanfar, M., and Szostak, J. W. (1993) *Nature 364*, 550−553.
12. Burke, D. H., and Hoffman, D. C. (1998) *Biochemistry 37*, 4653−4663.
13. Burgstaller, A. T., and Famulok, M. (1994) *Angew. Chem., Int. Ed. Engl. 33*, 1084−1087.
14. Burke, D. H., and Gold, L. (1997) *Nucleic Acids Res. 25*, 2020−2024.
15. Majerfeld, I., and Yarus, M. (1994) *Nat. Struct. Biol. 1*, 287−292.
16. Zinnen, S., and Yarus, M. (1995) *Nucleic Acids Symp. Ser. 33*, 148−151.
17. Majerfeld, I., and Yarus, M. (1998) *RNA, 4*, 471−478.
18. Famulok, M. (1994) *J. Am. Chem. Soc. 116*, 1698−1706.
19. Connell, G. J., Illangesekare, M., and Yarus, M. (1993) *Biochemistry 32*, 5497−5502.
20. Geiger, A., Burgstaller, P., von der Eltz, H., Roeder, A., and Famulok, M. (1996) *Nucleic Acids Res. 24*, 1029−1036.
21. Thompson, M. J., Mekhalfia, A., Jakeman, D. L., Phillips, S. E. V., Phillips, K., Porter, J., and Blackburn, G. M. (1996) *Chem. Commun.*, 791−792.
22. Thompson, M. J., Mekhalfia, A., Hornby, D. P., and Blackburn, G. M. (1999) *J. Org. Chem. 64*, 7467−7473.
23. Frantzen, F., Faaren, A. L., Alfheim, I., and Nordhei, A. K. (1998) *Clin. Chem. 44*, 311−316.
24. Matzura, O., and Wennborg, A. (1996) *Comput. Appl. Biosci. 12*, 247−249.
25. Zuker, M., Mathews D. H., and Turner, D. H. (1999) in *A Practical Guide in RNA Biochemistry and Biotechnology* (Barciszewski, J., and Clark, B. F. C., Eds.) NATO ASI Series, Kluwer Academic Publishers, Dordrecht, The Netherlands.
26. Karlsson, R., and Fält, A. (1997) *J. Immunol. Methods 200*, 121−133.
27. Morton, T. A., and Myszka, D. G. (1998) *Methods Enzymol. 295*, 268−294.
28. Dange, V., Van Atta, R. B., and Hecht, S. M. (1990) *Science 248*, 585−588.
29. Kazakov, S., and Altman, S. (1992) *Proc. Natl. Acad. Sci. U.S.A. 89*, 7939−7943.
30. Knight, R. D., and Landweber, L. F. (1998) *Chem. Biol. 5*, R215−220.
31. Draper, D. E., and Misra, V. K. (1998) *Nat. Struct. Biol. 5*, 927−930.
32. Landweber, L. F., and Pokrovskaya, I. D. (1999) *Proc. Natl. Acad. Sci. U.S.A. 96*, 173−178.
33. Patel, D. J. (1997) *Curr. Opin. Chem. Biol. 1*, 32−46.
34. Chappey, O., Debray, M., Niel, E., and Scherrmann, J. M. (1994) *J. Immunol. Methods 172*, 219−225.

BI000295T